# Influence of post annealing treatments on the luminescence of rare earth ions in ZnO:Tb,Eu/Si heterojunction

*C. Guillaume[1], J.L. Frieiro[2], O. Blázquez[2], C. Labbé[1], J. López-Vidrier[2], B. Garrido[2], S. Hernández[2], B. Liu[3], L. Khomenkova[4,5], C. Frilay[1], F. Lemarié[1], C. Leroux[6], D. Pelloquin[6] and X. Portier[1]*

[1] CIMAP, CEA, UMR CNRS 6252, ENSICAEN, Normandie Université, 6 Boulevard du Maréchal Juin, 14050 Caen, France

[2] MIND-IN2UB, Departament d'Enginyeria Electrònica i Biomèdica, Universitat de Barcelona, Martí i Franquès 1, E-08028, Barcelona, Spain

[3] Shenyang National Laboratory for Materials Science (SYNL), Institute of Metal Research (IMR), Chinese Academy of Sciences (CAS), No. 72, Wenhua Road, Shenhe District, Shenyang, 110016, China

[4] V. Lashkaryov Institute of Semiconductor Physics of the NAS of Ukraine, 45 Prospect Nauky, 03028 Kyiv, Ukraine

[5]National University of "Kyiv-Mohyla academy", 2 Skovorody str., 04070 Kyiv, Ukraine

[6] CRISMAT, UMR CNRS 6508, ENSICAEN, Normandie Université, 6 Boulevard du Maréchal Juin, 14050 Caen, France

Corresponding author : clement.guillaume@ensicaen.fr

Keywords : Magnetron sputtering ; ZnO thin film ; (Tb, Eu)-co-doping ; Annealing ; Photoluminescence ; Electroluminescence

**Abstract**

(Tb, Eu)-co-doped ZnO films with about 3 at.% total doping rate were grown by magnetron sputtering on Si substrate. Post annealing treatments were performed at 973-1373 K in continuous nitrogen flow to investigate the transformation of microstructural and optical characteristics by means of X-ray diffraction, transmission electron microscopy, photoluminescence and electroluminescence. For annealing temperatures lower than 1073 K, segregation of Eu and Tb was observed mainly at the film/substrate junction. For temperatures higher than 1173 K, additional phases appeared, namely, $Zn_2SiO_4$ and rare earth silicates. For the highest temperature investigated (1373 K), only silica and rare earth silicates remained in the film due to Zn evaporation. PL measurements indicated a very intense Eu emission associated with the presence of rare earth silicate inclusions. Energy transfer from Tb towards Eu was evidenced in this secondary phase. At last, based on these results, an (Tb, Eu)-co-doped ZnO/Si electroluminescent structure was produced and showed very promising results paving the way for very thin ZnO based light emitting diodes.

## 1. Introduction

ZnO is a well-known wide band-gap (3.3–3.4 eV) semiconductor suitable for many applications in the optoelectronic industry such as optical sensors and light emitting diodes (LEDs) but also in other emerging fields [1]. Indeed, its attractive physical properties

combined with the fact that the ZnO growth is relatively simple at various scales using different growth techniques (sol gel [a], MOCVD [b], PLD [c], MBE [d], ALD [e], sputtering [10] methods for bulk and films and various chemical synthesis approaches where Zn salts are combined with bases) make this material the object of many studies during last decades. In addition, relevant doping can lead to interesting optical functionalities which are currently achieved with more expensive and/or hazardous materials such as indium tin oxide [f] or gallium nitride [g].

Rare earth (RE) doping is often linked to optical functionalities such as light emitting diodes for lighting or associated to energy conversion (down conversion, down shifting or up conversion) in photovoltaic structures. The photoluminescence (PL) effect is due to internal *d-f* electronic transitions in the RE elements and when they are present in a transparent matrix such as ZnO, optical properties may be exploitable. Among these lanthanides, much attention is paid to terbium (Tb) and europium (Eu). Most of the time, these lanthanides have predominantly a $3^+$ valence state in ZnO. Tb ions can also have a $4^+$ valence, but this latter does not lead to a radiative recombination [2]. Eu ions can ~~also~~ possess a $2^+$ oxidation state (EuO and $EuSiO_3$ phases) upon high annealing temperature, leading to an UV broad band emission [3]. $Eu^{2+}$ has been found in ZnO, but its PL signature is inefficient by contrast to that of the $Eu^{3+}$ counterpart [4].

In previous works, Tb doped ZnO films revealed that an energy transfer from ZnO host to $Tb^{3+}$ is possible and allows an optimal emission of $Tb^{3+}$ upon an annealing close to 873 K [4, 5]. Energy transfer from ZnO host to $Eu^{3+}$ is also possible via $Zn_i$ and $V_{Zn}$ defects [6] and annealing treatment at temperatures close to 873 K is improving this RE emission as well [7]. However, these energy transfers are often qualified in the literature as non-efficient [7, 8]. Very recently, a ~~complete~~ study of ZnO:Tb (3 at.%), Eu (<1 at.%)/Si and ZnO:Tb (3 at.%), Eu (<1 at.%)/alumina films of about 800 nm thick and annealed at 1173 K has been performed [9]. The authors demonstrated the formation of Tb oxide at the grain boundaries between the ZnO columns (columnar growth) within the film and the formation of zinc silicate and rare earth silicate at the bottom of the film in the case of the Si substrate. No aluminate phase was observed in the annealed structure grown on the alumina substrate. Two families of PL peaks were identified: a broader one coming from the Tb oxide inclusions and sharper ones originating from the rare earth silicates. An energy transfer from Tb towards Eu was also mentioned.

Regarding ZnO:Tb,Eu films, a study on anneal treatments up to 1373 K was carried out revealing a very intense emission of $Eu^{3+}$ upon the anneal treatment at the highest temperature [10]. An explanation is given by an efficient energy transfer from $Tb^{3+}$ to $Eu^{3+}$ in a matrix of Willemite ($Zn_2SiO_4$). As mentioned in previous works performed on ZnO:RE layers, upon annealing, most of the lanthanides tend to diffuse out of the ZnO matrix and created secondary phases inside the film at high temperatures (from 1173 K) [11]. This diffusion process occurs already for a few hundreds of degrees Celsius. But only a few studies dealt with the behavior of Tb and Eu doped ZnO thin films (about 150 nm thick) deposited on Si and submitted to extreme temperatures (up to 1373 K). The purpose of this work is to bring more insight on the various phases formed in doped ZnO films upon post anneal treatments and their associated luminescence properties. A complete study of the evolution of microstructural and optical properties with the annealing temperature for (Tb, Eu)-co-doped ZnO/Si junction will be presented. For the highest annealing temperature, an extreme chemical composition variation and structure modification is induced in the film. X-ray diffraction, transmission electron microscopy and energy dispersive X Ray spectroscopy

will be used for microstructural characterizations and photoluminescence measurements will be analyzed to understand the origin of the observed emissions as well as their evolution with the annealing temperature. A special attention will be focused on the microstructural evolution of the film and their consequences in the PL response and in particular for the highest annealing temperature where a new phase is obtained.

The efficiency of PL emission of rare earths in ZnO is usually low, but ZnO, being a rather good conducting oxide, offers another perspective such as the electrical excitation of RE doped ZnO-based junctions. Due to the presence of a significant amount of RE dopants at the level of the junction upon moderate thermal treatments, ZnO:Tb,Eu/Si junction could be an interesting structure for electroluminescence (EL). In this paper, a LED structure based on Tb and Eu doped ZnO/Si materials is also considered to determine whether a 150 nm doped ZnO film with only a few at.% doping grown on an Si substrate could be feasible. If this is the case, in principle, by producing a stack of three layers respectively doped with different RE elements providing red, green and blue emissions, a white LED structure could be achieved and could pave the way to a cheap structure for lighting functionalities.

## 2. Experimental details

The films were elaborated by a bottom-up radio frequency magnetron sputtering setup equipped with two separate targets and temperature controlled 2-inch wafer holders. All the films were grown on (001) oriented Si substrates (2 inch wafers). Film deposition was performed using argon plasma, a chamber vacuum pressure of 15 µbar, a power density fixed at 1.95 W $cm^{-2}$ and a substrate temperature value of 373 K. The holder/target distance was set at 7 cm. The target was composed of a pure 4 inch ZnO target on the top of which 4 $Tb_4O_7$ and 10 $Eu_2O_3$ calibrated pellets were placed. Several preliminary experiments were carried out in order to correlate the number of pellets with the corresponding doping rate and the above mentioned configuration gave rise to 1.6 at.% and 1.3 at.% for Tb and Eu concentrations, respectively. These last values were obtained by energy dispersive X Ray (EDX) spectroscopy measurements in a JSM6400 JEOL scanning electron microscope for as deposited films of about 1.5 µm thick to make sure that the excited volume by the electron beam came only from the film and not from the substrate. Except for this specific measurement, all the films discussed in the photoluminescence study were 150 nm thick and the film dedicated to the electroluminescence experiment was 65 nm thick.

Wafers were cut in regular squared pieces (about 1 cm x 1 cm) and annealing treatments of the films were performed in a conventional furnace at $T°_A$ = 973-1373 K with a step of 100 K during 1h in a continuous nitrogen flow. The samples were left in the furnace for the cooling down to room temperature.

Microstructural investigations were conducted using X-ray diffraction and transmission electron microscopy (TEM) techniques. X-ray diffraction diagrams were acquired with a D8 Bruker Discover diffractometer, using a Cu ($\lambda_{K\alpha1}$ = 1.5406 Å) source, in Bragg Brentano configuration (θ-2θ). TEM observations in various modes were performed with a double corrected (probe and imaging) JEOL ARM200F microscope equipped with a cold FEG (Field Emission Gun) source operated at 200 kV. With this microscope, a point to point resolution of the order of 1.0 Å could be reached in high resolution mode (HRTEM). In addition, it was equipped with a scanning system (STEM) which offered the possibility to take chemical contrast images (resolution of 0.78 Å) owing to a high angle annular dark field (HAADF) detector as well as STEM EDX chemical mapping at a nanometer scale owing to a

CENTURIO JEOL EDX spectrometer. The thin foils for TEM observations were prepared by a focused ion beam system (FEI HELIOS NanoLab 660) and prior to the thinning with a gallium beam, the top surface of the film was protected with a thin carbon film (a few tens of nm thick) and two platinum layers, one deposited electronically and the final one grown with the ion beam (a few microns thick in total).

Regarding optical properties, three laser sources were chosen for photoluminescence measurements. A laser diode at 266 nm, an argon laser at 488 nm and a frequency-doubled Nd:YAG laser at 532 nm wavelength have been used. The power density values were 2.6 W $cm^{-2}$ and 50.9 W $cm^{-2}$ for the first two lasers, respectively. For the third one, the beam went through the objective of a microscope with a x50 magnification. The beam diameter was estimated at 0.87 µm. The density power was close to 410 kW $cm^{-2}$. Such a power density represents approximately a factor of 1.6 $10^5$ compared to the laser used for $\lambda_{excitation}$ = 266 nm (2.6 W $cm^{-2}$). Considering this high power density, preliminary measurements for low power densities were carried out by incrementing, using filters, from low power densities up to 410 kW $cm^{-2}$. These latter measurements showed that there was no local annealing effect of the beam on the excited part of the film. Finally, note that cathodoluminescence results were also obtained, but the very low signal recorded did not permit to present and analyse properly these data for all the annealing temperature values.

For electroluminescent experiments, electrical contacts were produced by the Department of biomedical and electronic engineering at the University of Barcelona (MIND-IN2UB). Top transparent and highly conductive contacts were composed of ZnO cylinders of 100 nm height and 0.5 mm diameter, deposited on the ZnO:Tb,Eu film via atomic-layer-deposition (ALD) with a substrate temperature of 473 K. The bottom contact deposited on Si was a 200 nm thick layer of Al. Current-voltage characteristic [*I(V)*] and electroluminescent spectra were realized using an Agilent B1500A semiconductor device analyzer for *I(V)* measurements. Electroluminescence spectra of the device were acquired through the microscope channel, in optical mode with a CCD camera.

## 3. Structural properties

### 3.1. X-ray diffraction characterization

Figure 1 shows XRD diagrams of ZnO:Tb (1.6 at.%), Eu (1.3 at.%) films for various annealing temperatures ($T°_A$) and focused on the peak position corresponding to the (0002) planes of ZnO. The reference value for bulk ZnO is indicated. A significant difference (about 0.48°) is observed between the angular positions of the (0002) peak for the as-deposited film and that of the reference. This shift means an increase of the c parameter of about 1.3 %. It can be noted that the (0002) peak of the as-deposited film is relatively broad. For the films annealed at 973 K and 1173 K, the angular deviations are about -0.07° and +0.08°, respectively, revealing a variation in the c parameter of about +0.19 % and -0.23 %, respectively. For $T°_A$ = 1273 K, the (0002) peak intensity falls down and disappears, in favor of a rhombohedral structure with the parameters a = b = 13.95 Å and c = 9.32 Å, consistent with Willemite $Zn_2SiO_4$ and the appearance of the corresponding (41-50) planes. Interestingly, for the highest temperature (1373 K) the ZnO and $Zn_2SiO_4$ signatures have disappeared.

The ZnO average grain size of the films, calculated using the Scherrer equation following the [0002] axis, increases with $T°_A$ from 21 nm for the as-deposited film, up to 23 nm for the 973 K annealed film and 40 nm for 1173 K.

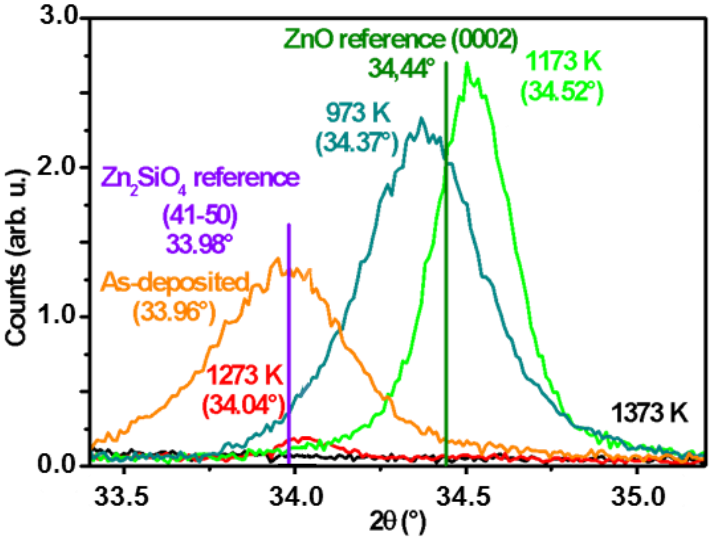


***Figure 1.*** *XRD patterns focused on the (0002) peak of ZnO recorded with Bragg-Brentano configuration (ϑ-2ϑ) of the ZnO:Tb,Eu films versus T°$_A$.*

Figures 2(a) and 2(b) are XRD diagrams of the same annealed ZnO:Tb,Eu films for the angular ranges from 21° up to 33° and from 39° up to 60°, respectively. For T°$_A$ = 1173 K, new peaks appear which are consistent with the above mentioned zinc silicate phase ($Zn_2SiO_4$). Another secondary phase is also detected by the presence of other peaks at 2θ = 21.82° ; 29.00° ; 31.82° ; 32.98° ; 39.90° ; 44.48° ; 48.72° ; 51.39° and 56.47°. These peaks are in good agreement with a rare earth silicate namely $Tb_xEu_ySi_vO_w$ in agreement with an apatite related phase. For the highest annealing temperature T°$_A$ = 1373 K, very sharp and intense peaks associated to this so called apatite related phase dominate the patterns whereas the peaks assigned to the $Zn_2SiO_4$ phase have disappeared. More details on this phase are given in the next section.

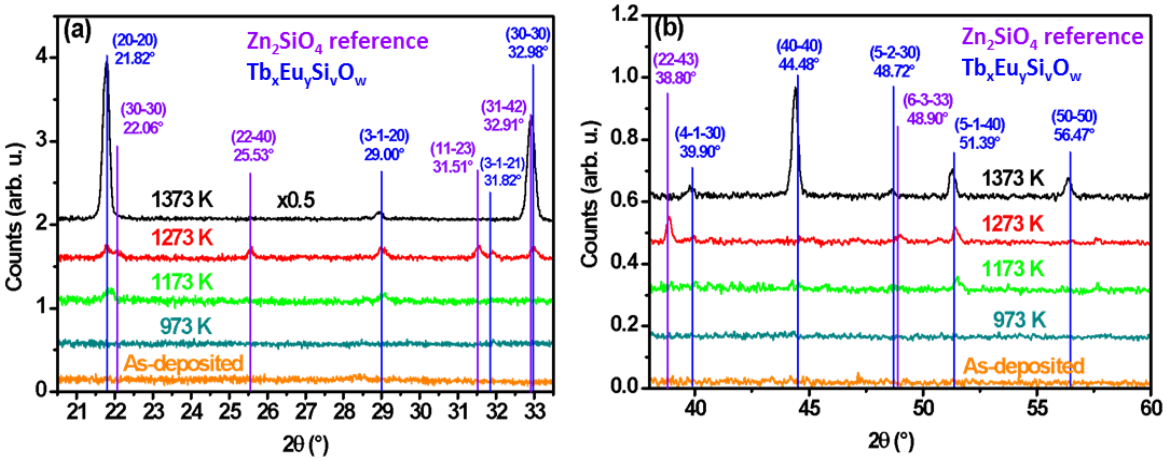


***Figure 2.*** *XRD patterns of the ZnO:Tb,Eu films for various T°$_A$ values and for the angular ranges from 20.5° to 33.5° (a) and from 36° to 60° (b).*

TEM observations have been carried to confirm these previous results at a nanoscale and to bring more details on the identification and localization of the RE silicate phase whose growth is generated upon thermal treatments from 1173 K.

### 3.2. Transmission electron microscopy observations

(Tb, Eu)-co-doped ZnO films, annealed at 973 K, 1273 K and 1373 K have been observed by TEM. Figure 3 summarizes some TEM images for the film annealed at 973 K. (a) and (b) images are bright field and high resolution (HR) TEM images, respectively. The Tb and Eu co-doped films have a typical columnar structure of wurtzite ZnO as shown in figure 3(a) by the elongated vertical Bragg and dark contrasts are observed. The HRTEM image is focused on the bottom part of the film, where two amorphous sublayers of a few nanometer thick with very different contrasts. The layer with the brighter contrast (about 3 nm thick) on the top of the substrate is a silica layer. The other thinner layer with a darker contrast located on top of the silica is enriched with Tb and Eu as demonstrated by the EDX chemical analysis. Figure 3(c) is a chemical profile of Tb and Eu following the line indicated in Figure 3(b). It clearly shows the RE enrichment over a thickness of about 4 nm at the bottom of the film just above the silica layer on the top of the Si substrate. Figure 3(d) shows an image taken in STEM HAADF mode with chemical contrasts. The uniform contrast across all the film except the bottom part suggests a uniform distribution of the species but chemical maps give more insight. At last, the two last illustrations in figures 3(e) and 3(f) are chemicals maps for Tb and Eu elements for the whole film confirming the segregation of the RE elements mainly at the bottom of the film over a thickness of about 3-4 nm.

This RE-enriched layer contains up to 5 at.% of Tb and 3 at.% of Eu. It results from the post-annealing diffusion of RE ions at the film/substrate interface. This diffusion creates a RE depleted zone, adjacent to the diffusion layer at the bottom of the film [figures 3(e-f)]. In the lower part of the film, diffusion forces linked to the potential well of the junction and/or the field of the space charge region of the junction stimulates the segregation of dopants towards the substrate during annealing [9]. Moreover, the lower part of the film close to the substrate has a lower grain size than the upper part of the film favoring REs diffusion [12]. The lower presence of RE in the rest of the film (upper part) seems homogeneous according to the homogeneous contrast of the Tb and Eu maps.

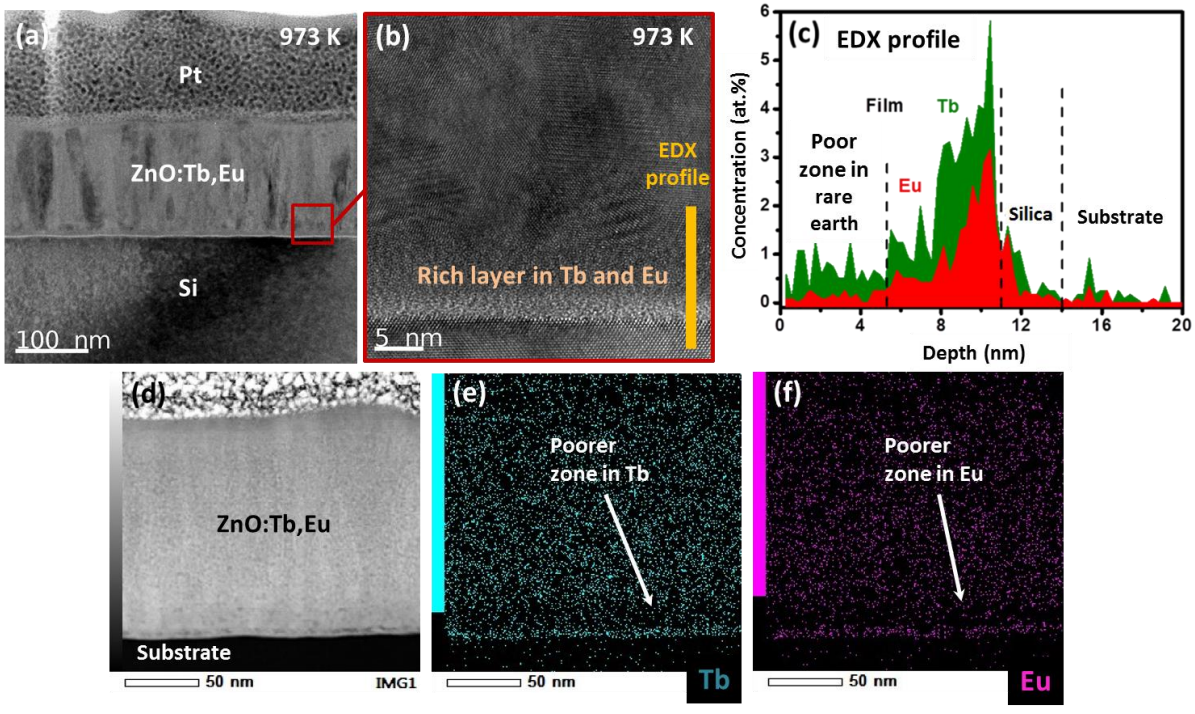


***Figure 3.*** *(a) Conventional TEM image and (b) high-resolution TEM image, of the ZnO:Tb,Eu,*

*film annealed at 973 K. (c) Chemical profile of Tb and Eu following the orange line in (b). (d) STEM HAADF image and EDX chemical maps for the Tb (e) and Eu (f) elements.*

Figure 4(a) is a cross-sectional view (bright field TEM image) of the ZnO:Tb,Eu film annealed at 1273 K, along the [110] direction of the Si substrate. One can observe the presence of a mostly crystallized phase at the bottom part of the film as evidenced by the darker Bragg contrasts in some regions and covering the whole film. Furthermore, the chemical maps in figures 4(c-g) show that this region of the film is composed of Zn, O and Si elements and it contains very few RE ions (0.6 at.% and 0.8 at.% for Tb and Eu, respectively). The presence of Si within the whole film (with about 16.0 at.%) is confirmed by figure 4(e). The formed phase in this bottom region has been identified by the analysis of various Fast Fourier Transformed (FFT) of high resolution TEM images as being $Zn_2SiO_4$ with a rhomboedral structure, the space group R-3 and the following lattice parameters $a = b =$ 13.95 Å and $c$ = 9.32 Å. This result is in agreement with the XRD data. In the upper part of the film, large grains of about 100 nm size with a darker contrast are easily visible. The chemical analysis of the inclusions reveals a high content of Eu (7.3 at.%) and Tb (12.2 at.%), as well as Si and O but a low content of Zn (figures 4(c-g)). The darker contrast is explained by the Bragg contrast (due to a crystalline phase) but also by a significant presence of RE (high Z value) in these inclusions.

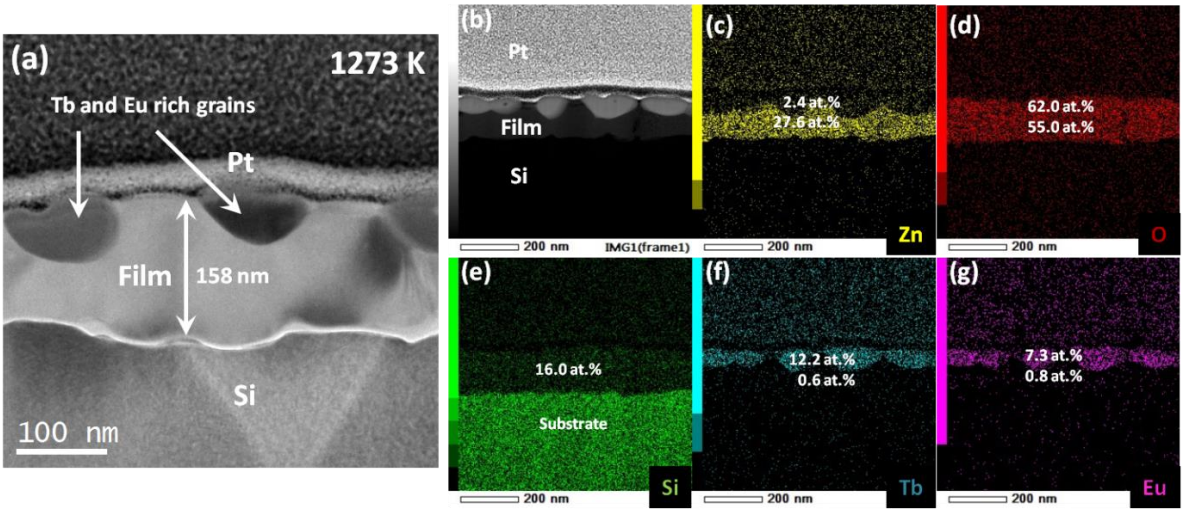


***Figure 4.*** (a) *Bright field TEM Image of the ZnO:Tb,Eu film for T°$_R$ = 1273 K. (c-g) Chemical maps of Zn (c), O (d), Si (e), Tb (f) and Eu (g), corresponding to the STEM HAADF image in figure (b).*

A typical bright field TEM image of the Tb and Eu silicate phase is presented in figure 5(a), showing two Tb and Eu rich grains (grains 1 and 2). Figure 5(b) is an HRTEM image of a region of grain 1. From different zone axes and their corresponding FFTs, as presented in figure 5(c) obtained from the high-resolution image of grain 1, a microstructural description can be made with a hexagonal apatite parent structure for the $Tb_xEu_ySi_zO_w$ phase, in agreement with the XRD data. Taking EDX data into account, the $Tb_{12,2}Eu_{7,3}Si_{16,0}O_{62,0}$ stoichiometry can be proposed for these inclusions.

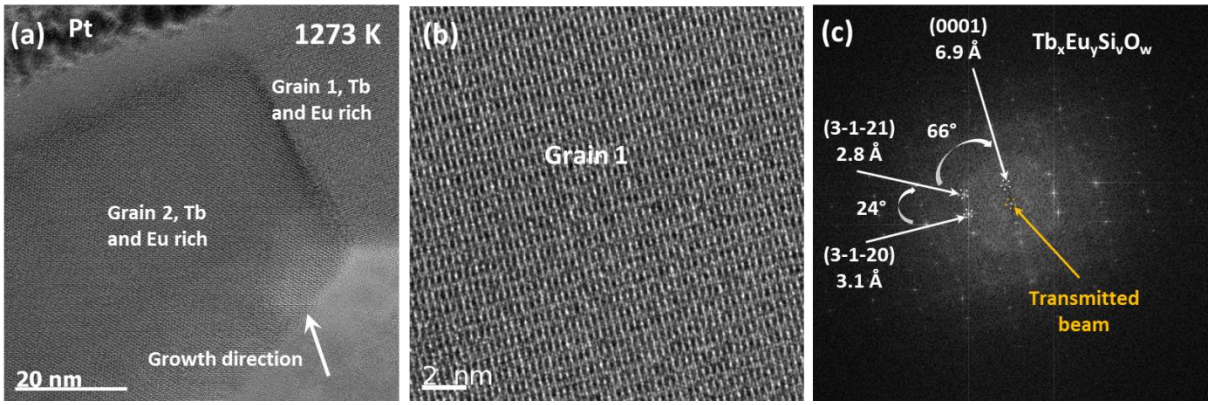


***Figure 5.*** *(a) Bright field TEM image of the ZnO:Tb,Eu film annealed at 1273 K showing two grains of a Tb and Eu rich phase localized at the upper part of the film. (b) HRTEM Image of grain 1, identified in figure 5(a). (c) Fast Fourier Transform of grain 1.*

A similar observation has been realized for the film annealed at 1373 K. In the TEM image in figure 6(a), the region of the film observed is composed of a grain with well-defined facets with an hexagonal shape, covering the entire thickness of the film (about 140 nm). Around this grain, an amorphous phase with a bright contrast is present. The data from the EDX maps shown in figures 6(d) and 6(e) give the following stoichiometry: $Si_{1,3}O_2$, which is close to silica for the amorphous phase with an additional 0.7 at.% of Zn, 1.1 at.% of Tb and 1.3 at.% of Eu. Moreover, crystallized $Zn_2SiO_4$ is also formed in the film (not visible in the presented region), in small proportion compared to the film annealed at 1273 K. As for the film annealed at 1273 K, the chemical analysis shows within the faceted grain, a significant amount of Tb of 11.0 at.% and Eu of 8.6 at.% as well as Si and O with 18.5 at.% and 61.0 at.%, respectively. These results reveal the evaporation of Zn upon extreme anneal treatment.

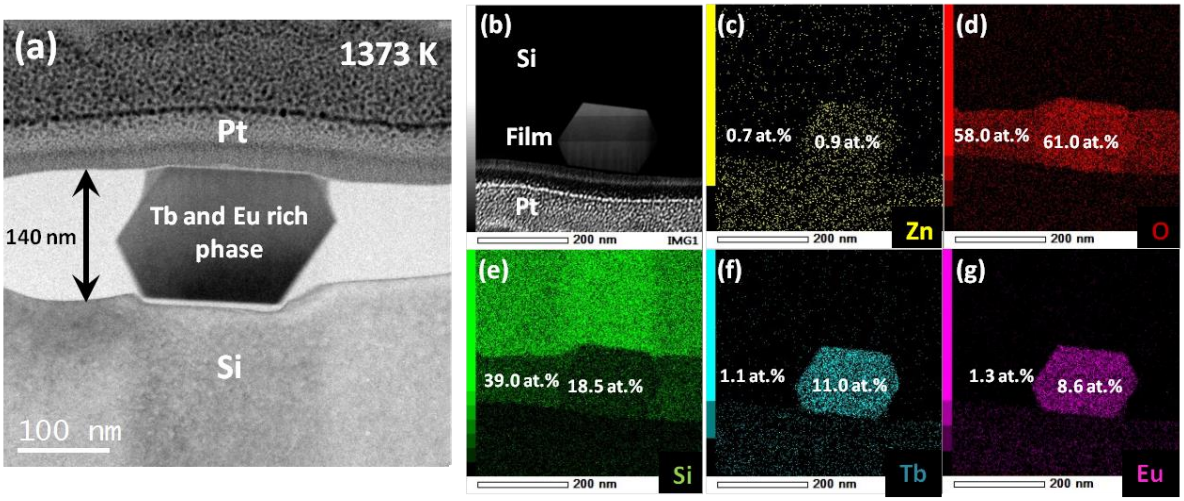


***Figure 6.*** *(a) Bright field TEM image for the ZnO:Tb,Eu film for $T°_A$ = 1373 K. (c-g) Chemical maps of Zn (c), O (d), Si (e), Tb (f) and Eu (g), corresponding to the STEM HAADF image in figure (b).*

Similarly to the previous annealing temperature, the $Tb_xEu_ySi_uO_w$ phase is identified from the FFT in figure 7(c) obtained from the high-resolution image of a part of the grain

shown in figure 7(b). Again, these data are consistent with an hexagonal structure crystallizing with the following cell parameters $a \approx b \approx 9.4$ Å and $c \approx 6.9$ Å close to an apatite-type structure. The phase stoichiometry is in favor of a Tb and Eu silicate with the following chemical formula : $Tb_{11,0}Eu_{8,6}Si_{18,5}O_{61,0}$. Note that a distortion of this hexagonal lattice is detected with the variation of the RE content (at 1373 K) as reported in a previous work on RE disilicate $RE_2Si_2O_7$ depending on the nature of the RE [13]. A more detailed study is in progress focused on the evolution of the RE silicates with the annealing temperature in these ZnO:Tb,Eu films and will be published in a forthcoming paper.

By comparison, the stoichiometry of the grains formed in the film annealed at $T°_A$ = 1273 K is relatively close to $Tb_{12,2}Eu_{7,3}Si_{16,0}O_{62,0}$. With the raise of $T°_A$ from 1273 K to 1373 K, the stoichiometry of this phase leads to a value of the [Tb]/[Eu] ratio which evolves from 1.67 down to 1.28. This latter value is close to 1.23 corresponding to the value of this ratio for the as-deposited film with an homogeneous distribution of the REs in the film. We conclude that for the extreme $T°_A$ value, the [Tb]/[Eu] ratio for the inclusions approaches the initial ratio.

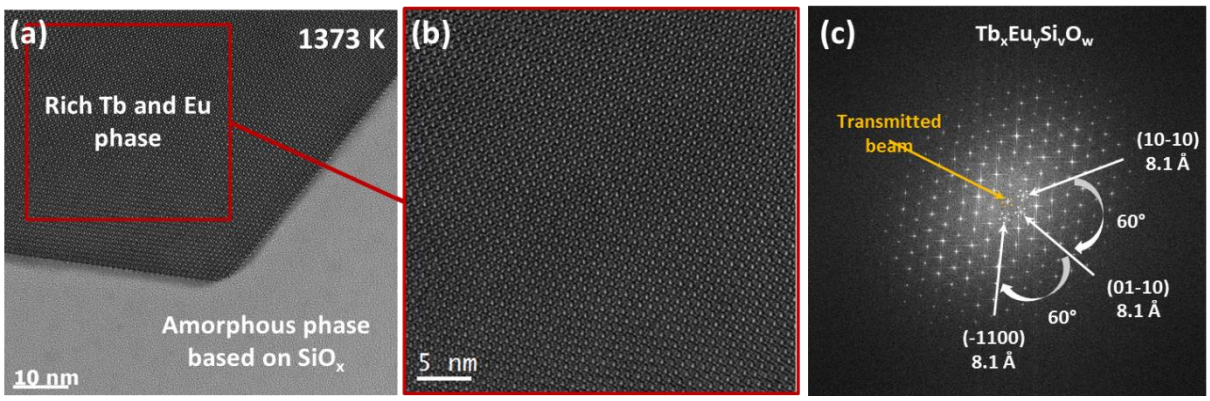


***Figure 7.*** *(a) HRTEM image of the ZnO:Tb,Eu film for $T°_A$ = 1373 K. (b) HRTEM Image from the squared region in red of the grain in figure (a). (c) Fast Fourier Transform associated to the grain in figure (b).*

### 3.3. Summary of the microstructural properties

The results demonstrate the diffusion of Tb and Eu and their segregation in an amorphous layer of a few nanometers thick at the film/substrate interface just above the native silica layer for $T°_A$ = 973 K. The formations of zinc silicate ($Zn_2SiO_4$) and apatite related ($Tb_xEu_ySi_uO_w$) inclusions are observed from $T°_A$ = 1173 K. These phases resulting from the diffusion of Si in the film supplant the main ZnO phase at lower $T°_A$ values. For $T°_A$ > 1173 K, the $Tb_xEu_ySi_uO_w$ phase becomes dominant within the film with grain sizes of a few hundred nanometers, while $Zn_2SiO_4$ tends to disappear in favor of silica and zinc evaporates almost completely from the film during annealing at the highest annealing temperature [14].

## 4. Photoluminescence properties

In this part, the PL properties of the films of ZnO:Tb,Eu are studied for different laser excitations and different $T°_A$ values. A particular attention is paid to the emission of the Tb

and Eu-based phases as well as to the interaction between these two dopants.
Although the positions of the Tb and Eu energy levels may fluctuate slightly from one matrix to another, an energy diagram is recalled in figure 8, for the trivalent ions of $Tb^{3+}$ and $Eu^{3+}$ in a $LaCl_3$ matrix [15]. The energy bands of ZnO are also specified. The three laser excitation wavelengths (532 nm, 488 nm and 266 nm) used are also displayed by colored arrows in order to highlight possible resonant levels with these excitations.

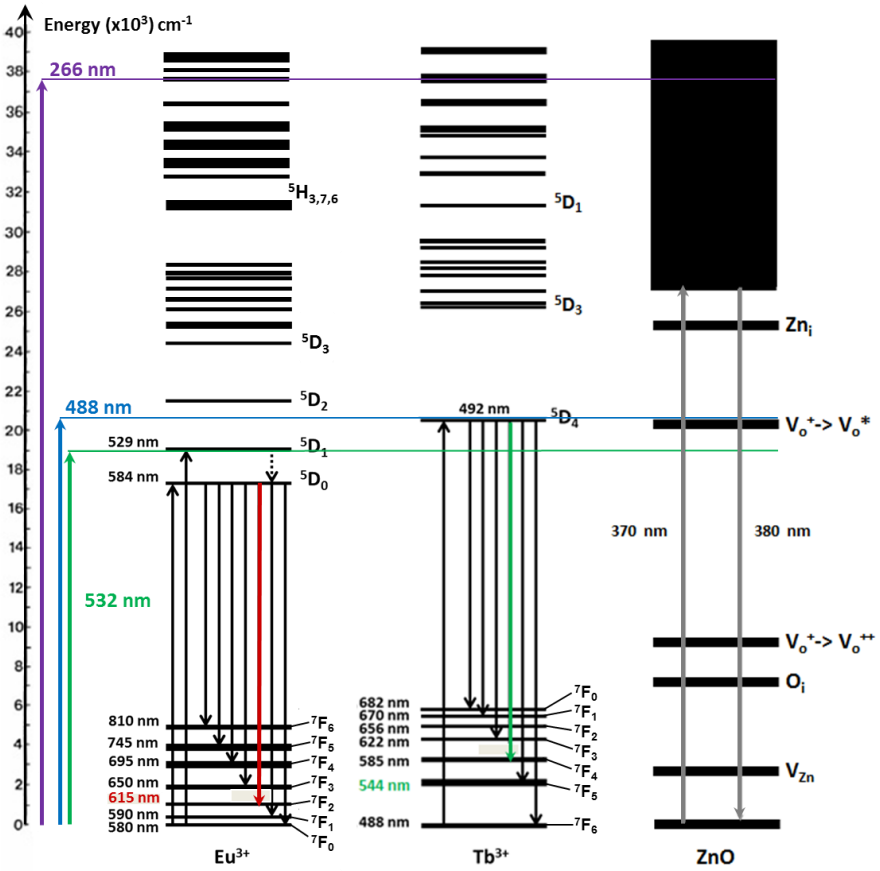


***Figure 8.*** *Energy diagram of $Eu^{3+}$ and $Tb^{3+}$(in $LaCL_3$), with the 532 nm (green), 488 nm (blue) and 266 nm (purple) excitations* [16]*. The energy diagram of ZnO defects is also presented for comparison* [17, 18].

Regarding the possible $Eu^{3+}$ positions in ZnO, some authors showed that $Eu^{3+}$ can replace $Zn^{2+}$ ions in the ZnO matrix and it is possible to excite $Eu^{3+}$ via the $Zn_i$ defects [19]. Other authors evoked the position of $Eu^{3+}$ in an interstitial position in the ZnO matrix [20, 21]. In addition, the large difference in ionic radius between $Zn^{2+}$ (0.74 Å) and $Eu^{3+}$ (0.91 Å) makes a substitution of $Eu_{Zn}$ difficult [22]. As far as $Tb^{3+}$ is concerned, the same types of positions (substitution of Zn [23, 24], interstitial site, and grain boundaries) and activations as for $Eu^{3+}$ are reported, via ZnO defects such as $Zn_i$ [25] or surface defects [22]. Indeed, $Tb^{3+}$ has an ionic radius close to 0.92 Å, close to that of $Eu^{3+}$, and much larger than that of $Zn^{2+}$ (0.74 Å). Thus, as for $Eu^{3+}$, the introduction of $Tb^{3+}$ in ZnO is possible, but subject to an instability which explains the phenomena of diffusion and segregation of these REs outside the structure of ZnO during heat treatments.

### 4.1. Laser excitation above the ZnO conduction band

The PL measurements of the ZnO:Tb (1.6 at.%), Eu (1.3 at.%) films as a function of the $T°_A$ are presented in figure 9, for a 266 nm excitation wavelength. Figure 9(a) shows the PL response for all $T°_A$ in the spectral range from 360 to 460 nm, whereas figures 9(b) and 9(c) display PL spectra in the 450 up to 750 nm spectral range for low (973, 1073 and 1173 K) and high $T°_A$ (1273 and 1373 K) values, respectively.

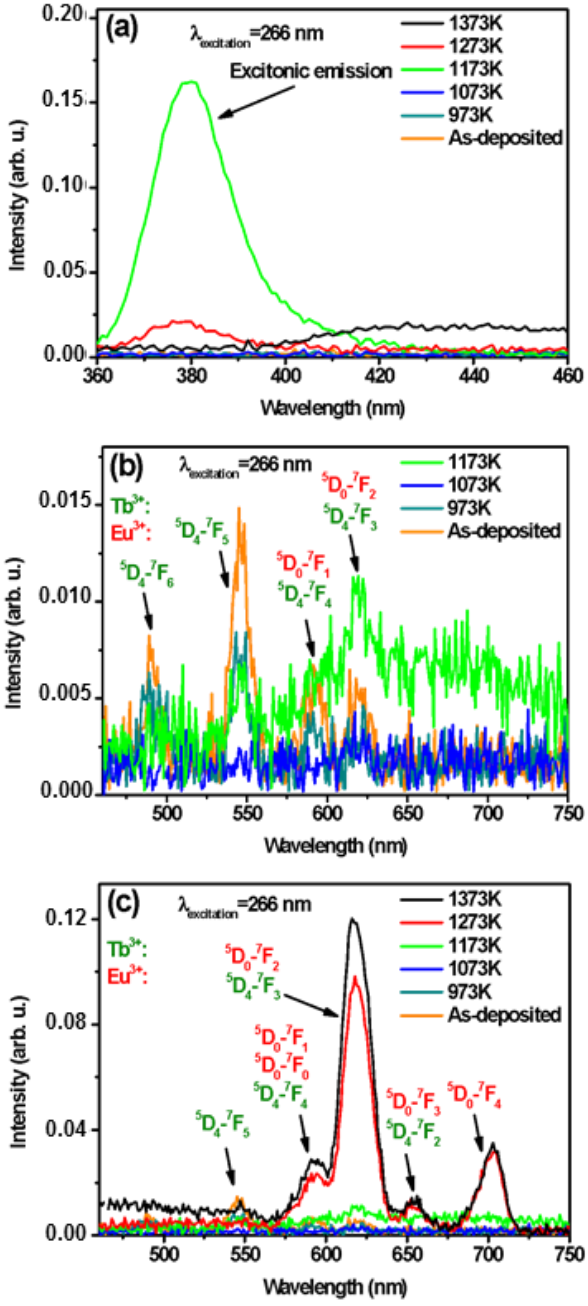


***Figure 9.*** *PL spectra of ZnO:Tb (1.6 at.%), Eu (1.3 at.%) film for a laser excitation at 266 nm, in the spectral range (a) from 360 to 460 nm and (b) from 460 to 750 nm for the lower annealing temperatures and (c) for all* $T°_A$.

*Indirect excitation of RE via ZnO defects :*

For an excitation upwards of the ZnO gap, figure 9(a) shows the presence of the excitonic peak emission for $T°_A$ = 1173 K (high intensity) and 1273 K (weak intensity). For the lowest $T°_A$ values, no emission is observed. For the highest $T°_A$ value at 1273 K and more clearly at 1373 K, the exciton peak collapses. As demonstrated in the previous section, the ZnO:Tb,Eu film reacts with the Si substrate to form zinc silicate ($Zn_2SiO_4$) and also Tb,Eu silicate ($Tb_xEu_ySi_vO_w$). It is therefore not surprising to see a drop of the excitonic emission of ZnO. For $T°_A$ = 1373 K (black curve), a wide band is visible from 380 nm to 460 nm, and even until 550 nm in figure 9(c). This latter cannot be associated with ZnO defects at such a $T°_A$ value since ZnO structure has totally disappeared. This broad emission band could come from the divalent ion $Eu^{2+}$ and its associated levels $4f^6 5d$ for which the emission wavelength is very sensitive to the crystal field [26, 27]. This emission of $Eu^{2+}$ could also have its origin in the formation of a metastable silicate of the $EuSiO_3$ type.

The PL intensity in the spectral range from 550 to 750 nm, corresponding to the defects in ZnO [figure 9(b)], is very low but observable for the film annealed at 1173 K. The main PL intensity peaks at 545 nm and 620 nm are those originating from the $Tb^{3+}$ and $Eu^{3+}$ ions, respectively (see figure 8). In this spectral range, the PL intensity is dominated by the $Tb^{3+}$ emission for the as-deposited and 973 K annealed films [figure 9(b)] while it mainly comes from the $Eu^{3+}$ ions for the highest annealing temperature [figure 9(c)].

This tipping of the PL intensity with high thermal budgets is explained as follows. The annealing generates the formation of the $Tb_xEu_ySi_vO_w$ phase and its presence seems to be at the origin of this high intensity of PL of $Eu^{3+}$ ions. However, it is possible that zinc silicate ($Zn_2SiO_4$) with Tb and Eu doping to the extent of 1 at.% for each RE, contributes in some extent to the emission of $Tb^{3+}$ and $Eu^{3+}$ [28]. However, the volume occupied by this phase tends to decrease drastically with the evaporation of Zn. At $T°_A$ = 1373 K, this phase is almost completely replaced by a silica phase with about 1 at.% of Tb and 1 at.% Eu doping [29], as noticed from XRD and TEM data, while the emission of $Eu^{3+}$ remains dominant with an increase of about 20 % (from $T°_A$ = 1273 K to 1373 K). The $Tb_xEu_ySi_vO_w$ phase whose grain size has increased with $T°_A$ [figures 4(a) and 6(a)] seems to be the main reason of this PL intensity evolution of $Eu^{3+}$.

Figure 10(a) connects the integrated PL intensities of $Tb^{3+}$ and $Eu^{3+}$ from 475 to 750 nm with the structural evolution of the matrix containing the emitting REs, with respect to $T°_A$. In figure 10(b), only the intensities at 545 nm ($Tb^{3+}$) and 620 nm ($Eu^{3+}$) are plotted as a function of $T°_A$. Note that for $T°_A$ = 1173 K, the PL signatures of the ZnO defects appear. We have subtracted these signals to keep only the integrated PL intensity of the REs.

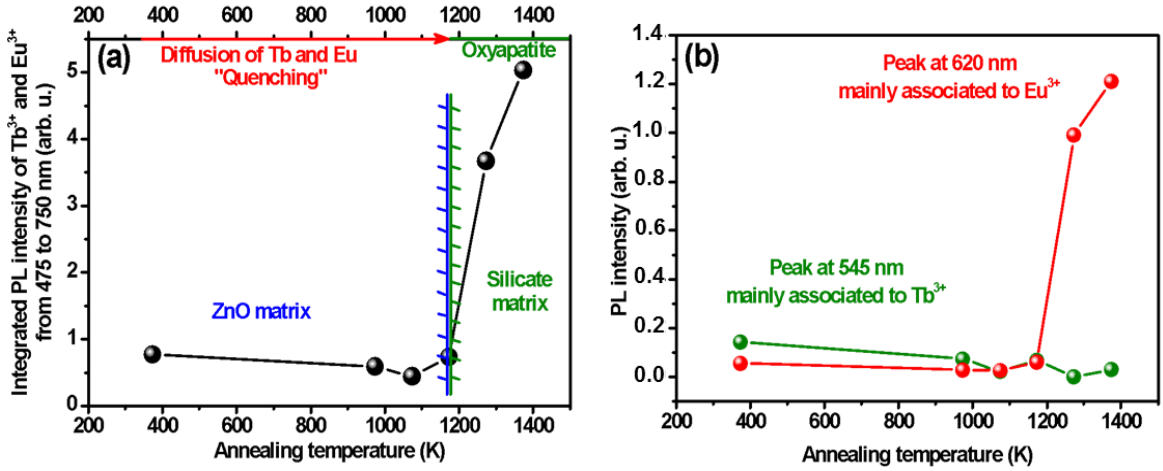


***Figure 10.*** *(a) Plot of integrated PL from 475 to 750 nm and (b) emission intensities at 545 nm and 620 nm versus $T°_A$ based on the PL spectra in figures 9(b and c) for an excitation at 266 nm.*

The plot in figure 10(a) shows a slight decrease in the integrated intensity from 373 K to 1073 K followed by a sudden and abrupt increase from 1073 K to 1373 K. Figure 10(b) discriminates the evolution of the two PL peak intensities of Tb and Eu : the intensity of the main emission peak of $Tb^{3+}$ (545 nm) decreases with $T°_A$ and the main emission peak of $Eu^{3+}$ (620 nm) increases suddenly for $T°_A$ > 1173 K. Note that the $^5D_4$-$^7F_3$ transition of $Tb^{3+}$ can also contribute to the intensity of the peak at 620 nm but in a much lesser extent.

*From $T°_A$ = 373 K to 1073 K :*

The visible emission is governed by the signal from $Tb^{3+}$ and more particularly, for the as-deposited film and with the increase of $T°_A$ until 1073 K this intensity decreases (figure 10(b)). It does not appear any $Eu^{3+}$ emission for such $T°_A$ values. The ZnO matrix is not conducive to an excitation of $Eu^{3+}$ [4, 30].

For the lowest $T°_A$ values down to 1073 K (blue field in figure 10(a)), the REs are mainly located within the host matrix. A homogeneous RE distribution, in particular for the as-deposited film would favor the emission of $Tb^{3+}$. At low $T°_A$, the $Tb^{3+}$ could be more excited via the ZnO defects than in the case of $Eu^{3+}$. On the other hand, with the increase of $T°_A$, the REs tend to diffuse from the ZnO matrix via the grain boundaries first and then towards the film/substrate interface [31]. The PL intensity of $Tb^{3+}$ tends to decrease with the annealing temperature, probably in relation with the RE diffusion phenomena observed in TEM at the bottom part of the film until $T°_A$ = 1073 K (from 373 K to 1073 K) leading to a quenching of the PL intensity of $Tb^{3+}$. This quenching is possibly induced by resonant non-radiative energy transfers [32] between $Tb^{3+}$ ions due to their proximity. They excite each other and increase the probabilities of non-radiative recombinations due to the segregation of the species in an amorphous environment. An oxidation of $Tb^{3+}$ to $Tb^{4+}$ can also be considered as mentioned by some authors [2]. These $4^+$ valence ions are known in the literature to not lead to a radiative emission and could be responsible for the disappearance of the luminescence of $Tb^{3+}$ linked to its wide and strong absorption band in the visible region.

*$T°_A$ = 1173 K :*

We note for $T°_A$ = 1173 K that the emission of the main peak of $Tb^{3+}$ is observable at 545 nm. However, another peak around 620 nm of the same intensity is also observed

[figure 9(b)] which is normally a less intense peak for $Tb^{3+}$. This difference in intensity may be due to a change in the environment around $Tb^{3+}$ favoring both the emissions of the $^5D_4$-$^7F_5$ and $^5D_4$-$^7F_3$ transitions of $Tb^{3+}$. But it is more likely that this emission is associated with the $^5D_0$-$^7F_2$ transition of $Eu^{3+}$ at 620 nm which is the main peak intensity of $Eu^{3+}$. This last hypothesis is supported by shorter distances between REs by diffusion of $Tb^{3+}$ and $Eu^{3+}$ towards the interfaces with the increase of $T°_A$ which leads to an activation of $Eu^{3+}$ by an energy transfer from $Tb^{3+}$ to $Eu^{3+}$ [33]. More importantly, it is most probable that the silicate phase described in the structural properties sections and containing relatively high amount of REs ($Tb_xEu_ySi_vO_w$) starts to form and leads to the emission of the REs in a favorable crystal field. The atomic arrangement in the lattice imposes certain specific distances between Tb and Eu which are most probably in favor of an energy transfer from Tb towards Eu.

*$T°_A$ > 1173 K :*

For $T°_A$ = 1273 K and 1373 K, the disappearance of ZnO and the increasing presence of the $Tb_xEu_ySi_vO_w$ phase are clearly demonstrated. In this phase, Tb and Eu are in relatively large quantities and the proximity of these two REs (with precise and periodic distances in the oxyapatite lattice) within the crystallized inclusions leads to an emission of $Eu^{3+}$ about 10 times more intense than its $Tb^{3+}$ counterpart. This configuration suggests an efficient energy transfer from $Tb^{3+}$ to the benefit of $Eu^{3+}$ within these $Tb_xEu_ySi_vO_w$ crystallites.

*Direct or indirect excitation of RE :*

Unfortunately, the low RE emissions in ZnO ($T°_A$ < 1073 K) do not allow PLE measurements to successfully determine and confirm the origin of the RE excitation. Therefore, it is difficult to determine whether there is a dominant indirect excitation of RE via ZnO host matrix (via ZnO defects) or a direct excitation of RE upon optical stimulation. Cathodoluminescence experiments (not shown) did not permit either to discriminate an excitation process, because of the high energy excitation. However, we can notice that a direct excitation of $Tb^{3+}$ and $Eu^{3+}$ at 266 nm is possible, as we can see it in the energy diagram of $Tb^{3+}$ and $Eu^{3+}$ in $LaCl_3$ (figure 8) and according to the work of Pavitra et al. [34]. The absorption of $Tb^{3+}$ occurs at the 4f-5d band. For Eu ions, an absorption band also exists in blue/UV linked to $Eu^{2+}$ which can lead to a broad emission bands between 250 and 550 nm. Another sharper absorption band between 200 nm and 350 nm is associated with the charge transfer from $O^{2-}$ to $Eu^{3+}$, which can cause emission of $Eu^{3+}$. Energy transfers between the bands of $Eu^{2+}$ to those of $Eu^{3+}$-$O^{2-}$ are also possible [26].
At last, the $Tb_xEu_ySi_vO_w$ phase seems to create a favorable path for absorption at 266 nm and the transfer of this energy to the energy states of $Tb^{3+}$, $Eu^{3+}$ and possibly $Eu^{2+}$ in a lesser extent, for which the emissions are observed [35].

### 4.2. Laser excitations below the ZnO conduction band

To further investigate the RE excitation process, a 532 nm excitation source was also used to characterize the PL emission of the films and more specifically the emission of $Eu^{3+}$ with the variation of $T°_A$. Indeed, according to the energy diagram of $Tb^{3+}$ and $Eu^{3+}$ in figure 8, it appears at a first glance that for an excitation wavelength of 532 nm, only the transition from the fundamental level $^7F_0$ of the $Eu^{3+}$ to the $^5D_1$ level can be directly excited [36].
The result of the PL measurements for the ZnO:Tb,Eu films as a function of $T°_A$ are presented

in figure 11. The spectral range detection is limited by our experimental system from 570 nm to 850 nm.

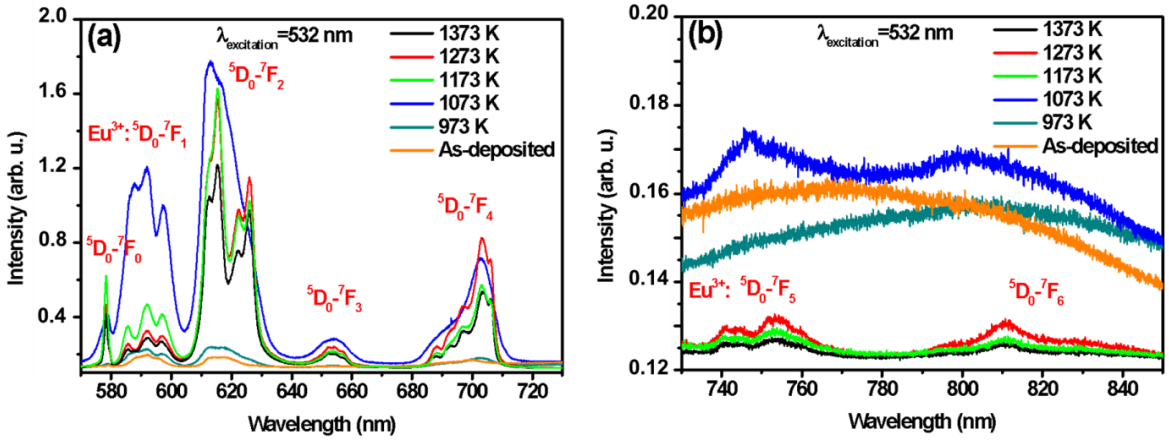


***Figure 11.*** *PL spectra from 570 nm to 730 nm (a) and from 730 nm to 850 nm (b) of ZnO:Tb,Eu films annealed at various T°$_A$ for a laser excitation at 532 nm.*

We can observe the unique emission of $Eu^{3+}$ due to the direct excitation at 532 nm. $Tb^{3+}$ is unlikely playing a role in the emission of the PL spectra in figures 11(a, b). Surprisingly, the emission of $Eu^{3+}$ increases overall with T°$_A$ and reaches a maximum at 1073 K. For higher T°$_A$ values, its intensity decreases gradually and seems to remain stable for T°$_A$ = 1273 K and 1373 K with a better signature (sharper peaks) of the $Eu^{3+}$ emission.

The $Eu^{3+}$ ions present in ZnO for the values of T°$_A$ < 1173 K are therefore optically active even in the as-deposited film. Because of the diffusion and segregation processes, $Eu^{3+}$ ions are mostly present at the bottom of the film in solid solution without forming secondary phases and a small amount is still present in the matrix. All $Eu^{3+}$ ions contribute to the signal and the rising in the emission intensity of $Eu^{3+}$ with T°$_A$ is most probably induced by the improvement of the crystalline quality of the ZnO matrix which reduces the non-radiative recombination mechanisms by the passivation of defects.

Beyond, for T°$_A$ = 1173 K, 1273 K and 1373 K, the overall PL intensity saturates and decreases slightly. This decrease in intensity could be due to the lower volume of the REs rich inclusions compared to the whole volume of the film. Furthermore, for these annealing temperatures, the peaks are better defined revealing the different contributions of the sub-energy levels of the same multiplet. The observation of this fine structure of the emission is rarely achievable at room temperature, since the difference between these energy levels is less than the thermal energy, $k_BT$ = 25 meV. The power density of 410 kW.cm$^{-2}$ and the relatively high emission intensity may explain the observation of these peaks. Observing a change in the shape of these narrow peaks as a function of T°$_A$, seems to indicate a modification of the local environment around the $Eu^{3+}$ and particularly, a different and better crystallized environment. Indeed, the environment of these ions went from a ZnO matrix (in the grains and/or at grain boundaries) for the lowest T°$_A$ values, to a silicate matrix such as the $Tb_xEu_ySi_vO_w$ phase offering better conditions for the emission of RE elements.

### 4.3. Highlight of an energy transfer from $Tb^{3+}$ to $Eu^{3+}$

This part comes back on the energy transfer mechanism between $Tb^{3+}$ and $Eu^{3+}$ in the $Tb_xEu_ySi_vO_w$ phase in order to highlight it in more detail. Indeed, from an excitation at 488

nm (with a power density of 50.9 W.cm$^{-2}$), it is possible to excite $Tb^{3+}$ from the fundamental level $^7F_6$ to the $^5D_4$ excited level only. The $Eu^{3+}$ excitation seems to be unlikely in this configuration [37].

PL measurements using an excitation at 488 nm have been performed for the ZnO:Tb,Eu film annealed at 1373 K. The PL spectrum of this sample is presented in figure 12.

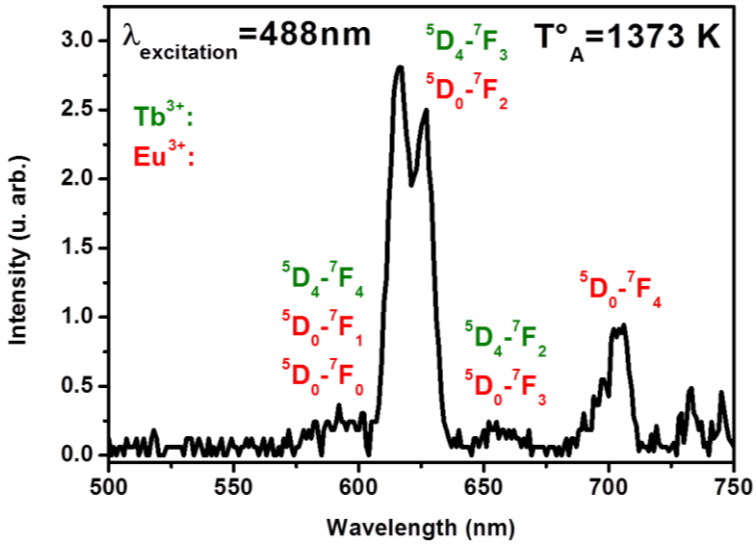


***Figure 12.*** *PL spectrum of the ZnO:Tb,Eu film annealed at 1373 K for a laser excitation at 488 nm.*

Despite the direct excitation of $Tb^{3+}$, no signal associated with this RE is recorded between 500 and 750 nm, not even the main emission of $Tb^{3+}$ which is usually located around 544 nm, as it can be observed in figure 9(b). On the other hand, a strong emission of $Eu^{3+}$ is observed. It is centered mainly at about 620 nm and 700 nm. It occurs from the $^5D_4$-$^7F_4$ (585 nm) and $^5D_4$-$^7F_5$ (544 nm) transitions of $Tb^{3+}$ to the $^7F_0$-$^5D_0$ (580 nm) and $^7F_0$-$^5D_1$ (535 nm) transitions of $Eu^{3+}$ [10, 38]. Such a total energy transfer, apparently very efficient in the $Tb_xEu_ySi_vO_w$ phase from $Tb^{3+}$ to $Eu^{3+}$ was similarly observed (not shown) in a film containing 4.4 times more $Tb^{3+}$ than $Eu^{3+}$.

### 4.4. Summary of the PL properties

In ZnO the RE ions PL emissions are globally weak caused by a low solubility of RE elements in this matrix [39]. The $Tb^{3+}$ emission is the only RE emission observed in ZnO but it decreases when increasing $T°_A$ with the out-diffusion from ZnO grains. From $T°_A$ = 1173 K, the $Tb_xEu_ySi_vO_w$ phase is forming, giving rise to a dominant $Eu^{3+}$ PL emission. The energy transfer from $Tb^{3+}$ to $Eu^{3+}$ was confirmed by direct excitation of $Tb^{3+}$ at 488 nm showing an efficient and total energy transfer from $Tb^{3+}$ to $Eu^{3+}$ in the $Tb_xEu_ySi_vO_w$ phase by contrast in ZnO matrix.

## 5. Light emitting diode

Considering the results presented above, a LED device has been achieved from the ZnO:Tb,Eu/Si(n) structure annealed at 973 K. Indeed, for this $T°_A$ value, the best compromise between the quality of ZnO and the whole film structure is reached. The presence of a

significant amount of REs at the ZnO/Si junction and just above the thin silica layer is potentially favorable for an emitting source via electrical excitation. For higher $T°_A$, the relatively important volume of resistive silica and the inhomogeneous distribution of $Tb_xEu_ySi_vO_w$ inclusions in the film make difficult the elaboration of a LED device.

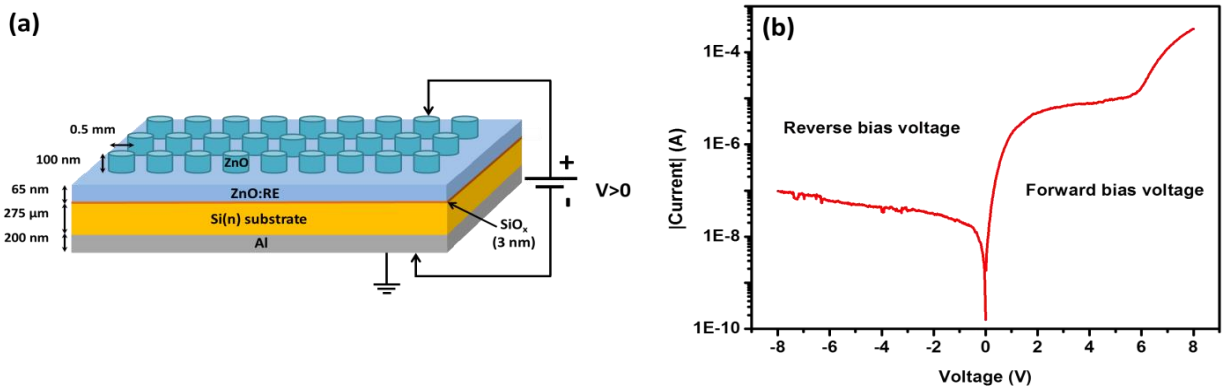


***Figure 13.*** *LED device based on the ZnO:Tb,Eu/Si(n) heterojunction annealed at 973 K in forward bias voltage (a) and the corresponding I(V) diode behavior (b).*

The ZnO:Tb,Eu layer used for the LED structure has a thickness of 65 nm. Al and ZnO materials have been used to obtain ohmic contacts on Si and ZnO:RE, respectively. The forward bias voltage is defined as shown in the diagram in figure 13(a). A typical diode behavior is observed for this device in figure 13(b).

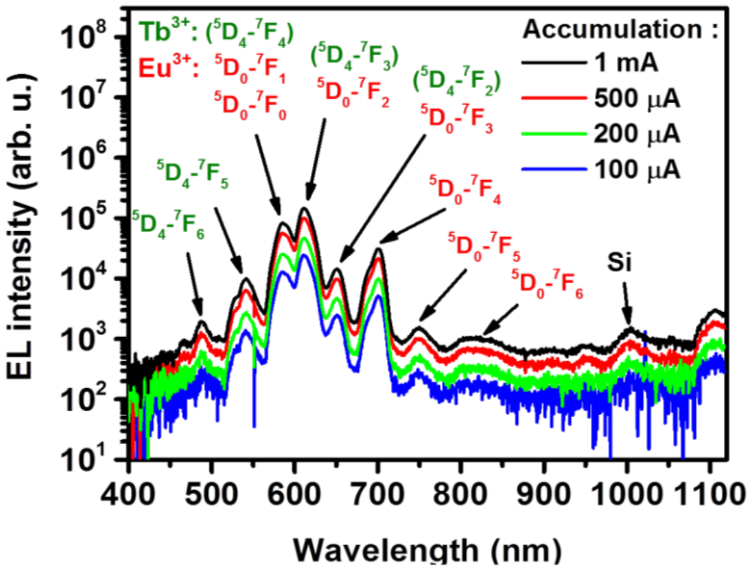


***Figure 14.*** *Electroluminescence spectrum of the ZnO:Tb,Eu/Si(n) junction annealed at 973 K.*

In figure 14 are recorded with success quite intense electroluminescence spectra of $Tb^{3+}$ and $Eu^{3+}$ obtained for various current values from 100 µA up to 1 mA in forward bias voltage. $Eu^{3+}$ emission is the most intense suggesting an energy transfer between the REs. RE excitation mechanism has been developed and discussed in a recently published paper [40].

## 6. Conclusion

150 nm thick ZnO films with Tb (1.6 at%) and Eu (1.3 at%) codoping rates have been produced successfully by radiofrequency magnetron sputtering on (100) oriented Si substrates and the effects of post annealing treatment at extreme temperatures have been studied. The temperature induced an out-diffusion of RE from matrix, an accumulation of RE at the film/substrate interface is observed. The temperature and the RE out-diffusion participate to an improvement of the crystalline quality (rises of the crystallized volume and c parameter shift closer to reference) of the ZnO matrix was observed between the as-deposited films and those annealed for $T°_A$ < 973 K. Regarding the photoluminescence properties, a weak emission of RE in ZnO has been noticed. It is explained by a difficult stable insertion of Tb and Eu into the ZnO matrix, due to their ionic diameters greater than $Zn^{2+}$. Therefore, they diffuse more easily at grain boundaries and at the film interfaces upon thermal treatments. For such low $T°_A$ values, only $Tb^{3+}$ is able to emit (for an excitation at 266 nm) but a phenomenon of quenching quickly appears when it diffuses and segregates at the bottom of the film without formation of secondary phases. The oxidation state from $Tb^{3+}$ to $Tb^{4+}$ leading to non-radiative recombinations may be the cause but further XPS measurements are necessary to confirm this assumption. $Eu^{3+}$ is optically active by direct excitation at 532 nm.

For higher $T°_A$ values up to 1373 K, the Si substrate reacts with the RE doped ZnO films, zinc silicate ($Zn_2SiO_4$) and $Tb_xEu_ySi_vO_w$ apatite related inclusions of a few hundreds of nanometers were identified by XRD and TEM observations. Zinc silicate tends to decrease in volume with increasing temperature as the zinc evaporates, leaving only RE silicate and silica in the film. A more detailed structural study is in progress to determine more precisely the observed ($Tb_xEu_ySi_vO_w$) structure. $Tb_xEu_ySi_vO_w$ phase is considered as the main emitting phase of our films. The PL spectrum is dominated by the $Eu^{3+}$ signal. The presence of $Eu^{2+}$ is also observed in PL (excitation at 266 nm) for $T°_A$ = 1373 K, as well as a weak $Tb^{3+}$ emission (excitation at 266 nm). Contrary to what was mentioned in previous works [10], it is most probable that zinc silicate doped with Tb and/or Eu plays a minor role in this emission because the RE contents in this phase is low (<1 at.%) and furthermore, this phase mostly disappears at 1373 K, with the concomitant Zn evaporation. A direct laser excitation of $Eu^{3+}$ at 532 nm, induced the higher ~~excitation~~emission intensity for ~~$Tb^{3+}$~~$Eu^{3+}$ in the $Tb_xEu_ySi_vO_w$ phase. And for a direct excitation at 488 nm of $Tb^{3+}$, a total energy transfer to $Eu^{3+}$ is attested in the $Tb_xEu_ySi_vO_w$ phase. The $Tb_xEu_ySi_vO_w$ phase obtained for the highest $T°_A$ is thus very interesting in terms of emission intensity for $Tb^{3+}$ and $Eu^{3+}$ and for the efficient energy transfer from $Tb^{3+}$ to $Eu^{3+}$. Therefore, this phase would be of considerable interest for an electroluminescent device. Unfortunately, in our case, the quality of the film is deteriorated upon high post annealing temperatures (presence of $Tb_xEu_ySi_vO_w$ inclusion embedded in a silica matrix) such that these films seem compromised for good conducting abilities. On the basis of these results, it would be necessary to deposit an homogeneous film of this phase while eliminating the formation of cavities and silica, electrically insulating. Finally, the films annealed at 973 K present a good compromise for electroluminescence applications. Indeed, for this temperature, we have a good structural quality of the matrix combined with a moderate diffusion of REs at the film/substrate interface. We have clearly shown that the presence of a relatively high concentrations of REs at the junction interface between *n*-type ZnO:RE and doped Si (without formation of secondary phases) can give rise to interesting excitation phenomena by injections of carriers.

## 7. Acknowledgements

The authors would like to thank the “Agence Nationale de la Recherche (ANR)” in the framework of the “Investissements d’Avenir” with the reference “ANR-11-EQPX-0020” for the financial support that allowed the use of the JEOL ARM200F microscope and the acquisition of an FEI FIB system (HELIOS Nanolab 660) for TEM sample preparations. This work was also financially supported by the Spanish Ministry of Economy and Competitiveness (Project No. TEC2016-76849-C2-1-R). J.L.F. acknowledges the subprogram “Ayudas para la Formación de Profesorado Universitario” (No. FPU16/06257) from the Spanish Ministry of Education, Culture and Sports for economical support. All the TEM results reported in this article fall within the scope of the CNRS Research Foundation IRMA (FR 3095).

## 8. References

[a] L. Znaidi, G. J. A. A. Soler Illia, S. Benyahia, C. Sanchez, et A. V. Kanaev, Oriented ZnO thin films synthesis by sol–gel process for laser application, Thin Solid Films, 428 (2003) 257-262.

https://doi.org/10.1016/S0040-6090(02)01219-1

[b] N. W. Emanetoglu, C. Gorla, Y. Liu, S. Liang, et Y. Lu, Epitaxial ZnO piezoelectric thin films for saw filters, Mater. Sci. Semicond. Process., 2 (1999) 247-252.

https://doi.org/10.1016/S1369-8001(99)00022-0

[c] A. Fouchet, W. Prellier, B. Mercey, L. Méchin, V. N. Kulkarni, et T. Venkatesan, Investigation of laser-ablated ZnO thin films grown with Zn metal target: A structural study, J. Appl. Phys., 96 (2004) 3228-3233.

https://doi.org/10.1063/1.1772891

[d] D. M. Bagnall, Y. F. Chen, M. Y. Shen, Z. Zhu, T. Goto, et T. Yao, Room temperature excitonic stimulated emission from zinc oxide epilayers grown by plasma-assisted MBE, J. Cryst. Growth, 184-185 (1998) 605-609.

https://doi.org/10.1016/S0022-0248(98)80127-9

[e] J. Lim et C. Lee, Effects of substrate temperature on the microstructure and photoluminescence properties of ZnO thin films prepared by atomic layer deposition, Thin Solid Films, 515 (2007) 3335-3338.

https://doi.org/10.1016/j.tsf.2006.09.007

[f] S.L. Ou, D.S. Wuu, S.P. Liu, Y.C. Fu, S.C. Huang, R.H. Horng, Pulsed laser deposition of ITO/AZO transparent contact layers for GaN LED applications, Optics Express 19 (2011) 16244-16251.

https://doi.org/10.1364/OE.19.016244

[g] M.S. Kang, C.H. Lee, J.B. Park, H. Yoo, G.C. Yi, Gallium nitride nanostructures for light-emitting diode applications, Nano Energy, 1 (2012) 391-400.

https://doi.org/10.1016/j.nanoen.2012.03.005

[1] M.A. Borysiewicz, ZnO as a functional material, a review, Crystals. 9 (2019) 505. https://doi.org/10.3390/cryst9100505

[2] R.K. Verma, K. Kumar and S.B. Rai, Inter-conversion of Tb3+ and Tb4+ states and its fluorescence properties in MO–Al2O3: Tb (M = Mg, Ca, Sr, Ba) phosphor materials, Solid State Sci. 12 (2010) 1146‑1151.

https://doi.org/10.1016/j.solidstatesciences.2010.04.004

[3] C. Panatarani, I.W. Lenggoro and K. Okuyama, The crystallinity and the photoluminescent properties of spray pyrolized ZnO phosphor containing Eu2+ and Eu3+ ions, Journal of Physics and Chemistry of Solids. 65 (2004) 1843–1847.

https://doi.org/10.1016/j.jpcs.2004.06.008

[4] C. Davesnne, Elaboration et caractérisation de films de ZnO dopé pour des applications optoélectroniques, PhD thesis, Université de Caen Basse Normandie, 2014.

https://hal.archives-ouvertes.fr/tel-01142121/file/These%20Christian%20DAVESNNE.pdf

[5] J. Zhang, H. Feng, W. Hao and T. Wang « Luminescent properties of ZnO sol and film doped with Tb3+ ion », Materials Science and Engineering : A. 425 (2006) 346–348.

https://doi.org/10.1016/j.msea.2006.03.082

[6] S.M. Ahmed, P. Szymanski, L.M. El-Nadi and M.A. El-Sayed, Energy-Transfer Efficiency in Eu-Doped ZnO Thin Films: The Effects of Oxidative Annealing on the Dynamics and the Intermediate Defect States, ACS Applied Materials & Interfaces, 6 (2014) 1765-1772.

https://doi.org/10.1021/am404662k

[7] Y. Terai, K. Yamaoka, K. Yoshida, T. Tsuji and Y. Fujiwara, Photoluminescence properties of Eu-doped ZnO films grown by sputtering assisted metalorganic chemical vapor deposition, Physica E. 42 (2010) 2834-2836.

https://doi.org/10.1016/j.physe.2010.03.012

[8] N. Korsunska, L. Borkovska, L. Khomenkova, O. Gudymenko, V. Kladko, O. Kolomys, V. Strelchuk, Z. Tsybrii, C. Guillaume, C. Labbe, X. Portier, O. Melnichuk and L. Melnichuk, Transformations in the photoluminescent, electrical and structural properties of Tb3+ and Eu3+ co-doped ZnO films under high-temperature annealing, Journal of Luminescence, 217 (2020) 116739.

https://doi.org/10.1016/j.jlumin.2019.116739

[9] N. Korsunska, L. Borkovska, L. Khomenkova, T. Sabov, O. Oberemok, O. Dubikovsky, Z.Ya. Zhuchenko, A. Zolotovsky, I.N. Demchenko, Y. Syryanyy, C. Guillaume, C. Labbe and X. Portier, Redistribution of Tb and Eu ions in ZnO films grown on different substrates under thermal annealing and its impact on Tb-Eu energy transfer, Appl. Surf. Sci. 528 (2020) 146913.

https://doi.org/10.1016/j.apsusc.2020.146913

[10] C. Davesnne, A. Ziani, C. Labbé, P. Marie, C. Frilay and X. Portier, Energy transfer mechanism between terbium and europium ions in zinc oxide and zinc silicates thin films, Thin Solid Films, 553 (2014) 33-37.

https://doi.org/10.1016/j.tsf.2013.11.122

[11] S.M.C. Miranda, M. Peres, T. Monteiro, E. Alves, H.D. Sun, T. Geruschke, R. Vianden, K. Lorenz, Rapid thermal annealing of rare earth implanted ZnO epitaxial layers, Optical Materials, 33 (2011) 1139-1142.

https://doi.org/10.1016/j.optmat.2010.10.009

[12] S. Hayamizu, H. Tabata, H. Tanaka and T. Kawai, Preparation of crystallized zinc oxide films on amorphous glass substrates by pulsed laser deposition, J. Appl. Phys. 80 (1996) 787‐791.

https://doi.org/10.1063/1.362887

[13] J. Felsche, Polymorphism and crystal data of the rare-earth disilicates of type RE2Si2O7, J. Common Met. 21 (1970) 1‐14.

https://doi.org/10.1016/0022-5088(70)90159-1

[14] X.Q. Zhao, C.R. Kim, J.Y. Lee, C.M. Shin, J.H. Heo, J.Y. Leem, H. Ryu, J.H. Chang, H.C. Lee, C.S. Son, B.C. Shin, J.W. Lee, W.G. Jung, S.T. Tan, J.L. Zhao and X.W. Sun, Effects of thermal annealing temperature and duration on hydrothermally grown ZnO nanorod arrays, Appl. Surf. Sci. 255 (2009) 5861-5865.

https://doi.org/10.1016/j.apsusc.2009.01.022

[15] G.H. Dieke and H.M. Crosswhite, The Spectra of the Doubly and Triply Ionized Rare Earths, Appl. Opt. 2 (1963) 675‐686.

https://doi.org/10.1364/AO.2.000675

[16] G.H. Dieke, Spectra and energy levels of rare earth ions in crystals, Interscience, 1968.

[17] S. Vempati, J. Mitra and P. Dawson, One-step synthesis of ZnO nanosheets: A blue-white fluorophore, Nanoscale Research Letters. 7 (2012) 470.

https://doi.org/10.1186/1556-276X-7-470

[18] C. Guillaume, Croissance, photoluminescence et électroluminescence de films de ZnO dopé terres rares, PhD thesis, Université de Caen Basse Normandie, 2020.

https://tel.archives-ouvertes.fr/tel-02499705/document

[19] Y. Zhang, Y. Liu, L. Wu, E. Xie and J. Chen, Photoluminescence and ZnO → Eu3+ energy transfer in Eu3+ -doped ZnO nanospheres, J. Phys. Appl. Phys. 42 (2009) 085106.

DOI:10.1088/0022-3727/42/8/085106

[20] P. Chen, X. Ma and D. Yang, ZnO:Eu thin films: Sol–gel derivation and strong photoluminescence from 5D0→7F0 transition of Eu3+ ions, J. Alloys Compound, 431 (2007) 317‑320.

https://doi.org/10.1016/j.jallcom.2006.05.078

[21] S. Zhao, F. Shu, Y. Li, C. Liu, W. Shan, Y. Cui and L. Yang, Synthesis and Luminescence Properties of ZnO:Eu 3+ Nano Crystalline via a Facile Solution Method, J. Nanosci. Nanotechnol. 12 (2012) 2607‑2611.

DOI:10.1166/jnn.2012.5761

[22] R.S. Ningthoujam, N.S. Gajbhiye, A. Ahmed, S.S. Umre and S.J. Sharma, Re-Dispersible Li + and Eu3+ Co-Doped Nanocrystalline ZnO: Luminescence and EPR Studies, J. Nanosci. Nanotechnol. 8 (2008) 3059‑3062.

DOI:10.1166/jnn.2008.152

[23] A. Hastir, R.L. Opila, N. Kohli, Z. Onuk, B. Yuan, K. Jones, Virpal and R.C. Singh, Deposition, characterization and gas sensors application of RF magnetron-sputtered terbium-doped ZnO films, J. Mater. Sci. 52 (2017) 8502‑8517.

DOI:10.1007/s10853-017-1059-9

[24] N.S. Singh, S.D. Singh and S.D. Meetei, Structural and photoluminescence properties of terbium-doped zinc oxide nanoparticles, Chin. Phys. B. 23 (2014) 058104.

DOI: 10.1088/1674-1056/23/5/058104

[25] V. Kumar, O.M. Ntwaeaborwa and H.C. Swart, Deep level defect correlated emission and Si diffusion in ZnO:Tb3+ thin films prepared by pulsed laser deposition, J. Colloid Interface Sci. 465 (2016) 295‑303.

https://doi.org/10.1016/j.jcis.2015.12.007

[26] X. Liu, W. Xie, Y. Lü, J. Feng, X. Tang, J. Lin, Y. Dai, Y. Xie and L. Yan, Multichannel Luminescence Properties of Mixed-Valent Eu2+/Eu3+ Coactivated SrAl3BO7 Nanocrystalline Phosphors for Near-UV LEDs, Inorg. Chem. 56 (2017) 13829‑13841.

https://doi.org/10.1021/acs.inorgchem.7b01938

[27] C.L. Heng, J.T. Li, Z. Han and P.G. Yin, An Abnormal Photoluminescence Enhancement in (Eu, Yb) Co-doped SiO2 Thin Film, Integr. Ferroelectr. 151 (2014) 179‑186.

https://doi.org/10.1080/10584587.2014.901125

[28] Q. Y. Zhang, K. Pita and C. H. Kam, Sol–gel derived zinc silicate phosphor films for full-color display applications, J. Phys. Chem. Solids. 64 (2003) 333‑338.

https://doi.org/10.1016/S0022-3697(02)00331-1

[29] G.H. Mhlongo, M.S. Dhlamini, O.M. Ntwaeaborwa, H.C. Swart and K.T. Hillie, Luminescent properties and quenching effects of Pr3+ co-doping in SiO2:Tb3+/Eu3+ nanophosphors, Opt. Mater. 36 (2014) 732‑739.

https://doi.org/10.1016/j.optmat.2013.10.031

[30] W. Jia, K. Monge and F. Fernandez, Energy transfer from the host to Eu3+ in ZnO, Opt. Mater. 23 (2003) 27‑32.

https://doi.org/10.1016/S0925-3467(03)00054-5

[31] H. Akazawa and H. Shinojima, Concentration effect of H/OH and Eu3+ species on activating photoluminescence from ZnO:Eu 3+ thin films, J. Appl. Phys. 114 (2013) 153502.

https://doi.org/10.1063/1.4825121

[32] G. Chen, F. Song, X. Xiong and X. Peng, Fluorescent Nanosensors Based on Fluorescence Resonance Energy Transfer (FRET), Ind. Eng. Chem. Res. 52 (2013) 11228‑11245.

https://doi.org/10.1021/ie303485n

[33] L. Luo, F.Y. Huang, G.S. Dong, H.H. Fan, K.F. Li, K.W. Cheah and J. Chen, Strong luminescence and efficient energy transfer in Eu3+/Tb3+-codoped ZnO nanocrystals, Opt. Mater. 37 (2014) 470‑475.

https://doi.org/10.1016/j.optmat.2014.07.008

[34] E. Pavitra, G.S.R. Raju, Y.H. Ko and J.S. Yu, A novel strategy for controllable emissions from Eu3+ or Sm3+ ions co-doped SrY2O4:Tb3+ phosphors, Phys. Chem. Chem. Phys. 14 (2012) 11296.

DOI: 10.1039/c2cp41722g

[35] B. Kaleli, M. Kulakci and R. Turan, Mechanisms of light emission from terbium ions (Tb3+) embedded in a Si rich silicon oxide matrix, Opt. Mater. 34 (2012) 1935‑1939.

https://doi.org/10.1016/j.optmat.2012.05.036

[36] Y.-C. Li, Y.-H. Chang, Y.-F. Lin, Y.-S. Chang and Y.-J. Lin, Synthesis and luminescent properties of Ln3+ (Eu3+, Sm3+, Dy3+)-doped lanthanum aluminum germanate LaAlGe2O7 phosphors, J. Alloys Compound. 439 (2007) 367–375.

https://doi.org/10.1016/j.jallcom.2006.08.269

[37] A.K. Bedyal, D.D. Ramteke, V. Kumar and H.C. Swart, Excitation wavelength and Eu3+/Tb3+ content ratio dependent tunable photoluminescence from NaSrBO3:Eu3+/Tb3+ phosphor, J. Mater. Sci. Mater. Electron. 30 (2019) 11714–11726.

https://doi.org/10.1007/s10854-019-01533-4

[38] T. Ishizaka, R. Nozaki and Y. Kurokawa, Luminescence properties of Tb3+ and Eu3+-doped alumina films prepared by sol-gel method under various conditions and sensitized luminescence, J. Phys. Chem. Solids. 63 (2002) 613–617.

https://doi.org/10.1016/S0022-3697(01)00201-3

[39] M. Huang, S. Wang, G. Wan, X. Zhang, Y. Zhang, K. Ou and Lixin Yi, Effect of co-doped Tb3+ ions on electroluminescence of ZnO:Eu3+ LED, Journal of Materials Science: Materials in Electronics. 29 (2018) 7213–7219.

https://doi.org/10.1007/s10854-018-8709-9

[40] J.L. Frieiro, C. Guillaume, J. López-Vidrier, O. Blázquez, S. González-Torres, C. Labbé, S. Hernández, X. Portier, B. Garrido, Towards a white LED based on rare earth-doped ZnO, Nanotechnology. 31 (2020) 465207.

https://doi.org/10.1088/1361-6528/abadc9